Structures 59 (2024) 105710

Contents lists available at ScienceDirect

Structures

journal homepage: www.elsevier.com/locate/structures

Axial compression performance of concrete-filled-steel tube flat columns with a large steel ratio

Hanqin Wang [a], Dianchun Xuan [a], Qing Jiang [a,b,*], Junqi Huang [a,b], Xun Chong [a,b]

[a] School of Civil Engineering, Hefei University of Technology, Anhui Province 230009, China
[b] Anhui Civil Engineering Structures and Materials Laboratory, Anhui Province 230009, China

ARTICLE INFO

Keywords:
Concrete-filled steel tube flat column
Axial compression performance
Finite element analysis
Design method

ABSTRACT

To prevent columns protruded from the inside wall, concrete-filled steel tube flat columns (CFSTFCs) with a large steel ratio were proposed in this study by limiting the sectional width and increasing the sectional height. The influence of the aspect ratio and thickness of the steel tube on the axial compression performance of CFSTFCs was investigated by axial compression tests for 12 CFSTFCs. The test results showed that two different failure modes, including a horizontal buckling ring with welding seam fracture and overall instability with local buckling in the sectional height direction, occurred in the tests. The axial load-carrying capacity and axial deformation ductility of CFSTFCs were enhanced with increasing thickness of the steel tube under the same aspect ratio. However, the axial deformation ductility of CFSTFCs gradually decreased with increasing aspect ratio. Furthermore, the Mander and Han Linhai confined concrete models were used to simulate the in-filled concrete in CFSTFCs to analyze the confinement effect from steel tube to in-filled concrete in CFSTFCs. Finally, the tested ultimate axial load-carrying capacity of CFSTFCs was compared with the different specifications to acquire the design method of CFSTFCs.

1. Introduction

Concrete-filled steel tube columns (CFSTCs) have been widely used due to their high load-carrying capacity and excellent deformation capacity. The in-filled concrete can be confined by the steel tube to enhance the compressive strength and ductility. Meanwhile, the steel tube is also supported by the in-filled concrete to delay the local buckling deformation. In particular, square and rectangular CFSTCs have received special attention due to the convenient connection between steel beams. Scholars have conducted a series of studies on square and rectangular CFSTCs [1–11]. The studied parameters mainly include the thickness of the steel tube, sectional aspect ratio, material strength, and sectional configuration.

Ibañez et al. [1] noted that increasing the thickness of the steel tube can enhance the confinement of the steel tube on in-filled concrete. Compared with the circular section, the square and rectangular CFSTCs show smaller axial load-carrying capacities under thin steel tubes. Han and Yang [2,3] noted that a larger sectional aspect ratio causes a smaller deformation capacity of rectangular CFSTCs under axial compression. Cai et al. [4] and Du et al. [5] showed that using high-strength steel and concrete materials can enhance the axial load-carrying capacity of square and rectangular CFSTCs, and the axial deformation capacity is influenced by the concrete strength. For the sectional configuration, compared with the traditional right angle corner, a larger corner radius can improve the confinement effect from the steel tube to in-filled concrete [6,7]. Sections with larger corner radii often appear in cold-formed CFSTCs [8,9]. Furthermore, round-ended rectangular CFSTCs were proposed and investigated [10,11]. Some existing specifications gave the design methods of the axial load-carrying capacity of CFSTCs [12–17].

Although CFSTCs possess excellent load-carrying capacity, a larger sectional size of CFSTCs is needed to satisfy the requirements of stiffness and load-carrying capacity in steel frame structures. Thus, the CFSTCs often protruded from the inside walls. In apartment buildings, this phenomenon significantly influences the inside space and aesthetics. To mitigate this problem, the sectional width of CFSTCs should be decreased. Zhang et al. [18–20] proposed concrete filled steel tube flat columns (CFSTFCs) and conducted a series of studies on the axial compression, eccentric compression and seismic performance of CFSTFCs. The sectional aspect ratio of the studied CFSTFCs is larger than 2.0. The analysis results showed that CFSTFCs with 2.0–3.0 aspect ratios and 6–8 mm steel tube thicknesses exhibit poor ductility. Therefore,

* Corresponding author at: School of Civil Engineering, Hefei University of Technology, Anhui Province 230009, China.
E-mail address: jiangq@hfut.edu.cn (Q. Jiang).

https://doi.org/10.1016/j.istruc.2023.105710
Received 28 August 2023; Received in revised form 20 November 2023; Accepted 3 December 2023
Available online 9 December 2023

Table 1
Detailed size of the CFSTFC specimens.

Specimen	$D \times B \times t$ (mm)	Length (mm)	D/B	Steel ratio (%)
C1	300 × 150 × 8	900	2	18.25
C2	300 × 150 × 10			23.63
C3	300 × 150 × 12			29.40
C4	300 × 150 × 14			35.61
C5	400 × 150 × 8	1200	2.67	16.60
C6	400 × 150 × 10			21.46
C7	400 × 150 × 12			26.65
C8	400 × 150 × 14			32.21
C9	450 × 150 × 8	1350	3	16.07
C10	450 × 150 × 10			20.75
C11	450 × 150 × 12			25.75
C12	450 × 150 × 14			31.11

Table 2
Test results of concrete material (unit: MPa).

Specimen	f_{cu}	Average f_{cu}	Average f_c
1	35.5	39.2	29.8
2	36.6		
3	44.0		
4	42.6		
5	39.5		
6	36.9		

Table 3
Test results of steel material.

t (mm)	E_s (GPa)	f_y (MPa)	f_u (MPa)
8	194.9	292.0	411.7
10	204.5	356.7	475.3
12	204.9	319.8	442.0
14	195.2	362.0	520.8

thin-walled CFSTCs or CFSTFCs have been used to construct special-shaped CFSTCs and composite shear walls [21–23]. Although special-shaped CFSTCs have better load-carrying capacity than CFSTFCs, the larger sectional height limits the advantages of steel frame structures, such as a larger span and insider space.

Based on the existing research, increasing the thickness of the steel tube can improve the load-carrying capacity and deformation capacity of CFSTCs. However, for the investigated CFSTFCs in reference [19], the thickness of the steel tube was less than 8 mm. Compared with CFSTFCs with smaller steel ratios, if CFSTFCs with larger steel ratios have better load-carrying capacity and deformation capacity, these CFSTFCs can be designed to carry force individually rather than constructing special-shaped CFSTCs. In this study, 12 CFSTFCs with 8 mm-, 10 mm-, 12 mm-, and 14 mm-thick steel tubes and 2.0–3.0 aspect ratios were designed to further investigate the axial compression performance of CFSTFCs. The steel ratio of the test specimen ranges from 16.07% to 35.61%. The failure mode, axial load-carrying capacity, and ductility of the specimens were discussed in detail by analyzing the test results. In addition, two different confined concrete models were selected to validate the confinement from the steel tube to in-filled concrete. Finally, the design methods of the axial load-carrying capacity of CFSTFCs in different specifications were validated.

2. Experimental program

2.1. Test specimens

A total of 12 CFSTFC specimens were designed. Each CFSTFC was constructed by welding steel plates. The sectional height (D), sectional width (B) and thickness of the steel tube (t) are listed in Table 1. The aspect ratio (D/B) of the test specimens was set as 2.0, 2.67, and 3.0. To prevent the effects of end conditions, the length of all the test specimens was three times the D value[2]. A steel plate with a thickness of 25 mm was welded at each end of the CFSTFCs to apply the axial load. The material strength of all steel plates was Q235 (Q235 means that the yielding strength of steel was 235 MPa). The material strength of the in-filled concrete was C30 (C30 means that the cubic compressive strength of the concrete was 30 MPa).

2.2. Material properties

Six cubic samples of concrete (100 mm × 100 mm × 100 mm) were tested to acquire the material properties of concrete. The cubic compressive strength (f_{cu}) of each sample is listed in Table 2. The f_{cu} is 0.95 times the compressive strength for the 100 mm × 100 mm × 100 mm cubic samples[24]. The characteristic concrete strength (f_c) is 0.76 f_{cu}. The elastic modulus of the concrete material is 32.4 × 10^3 MPa.

The steel material properties were tested by plate samples. The elastic modulus (E_s), yielding strength (f_y), and maximum strength (f_u) of steel plates with different thicknesses are shown in Table 3.

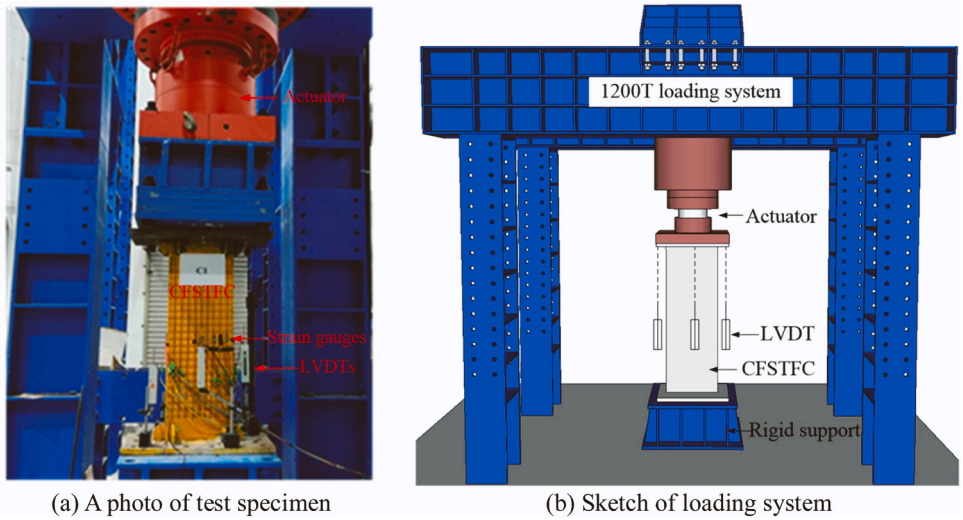

(a) A photo of test specimen (b) Sketch of loading system

Fig. 1. Test setup.

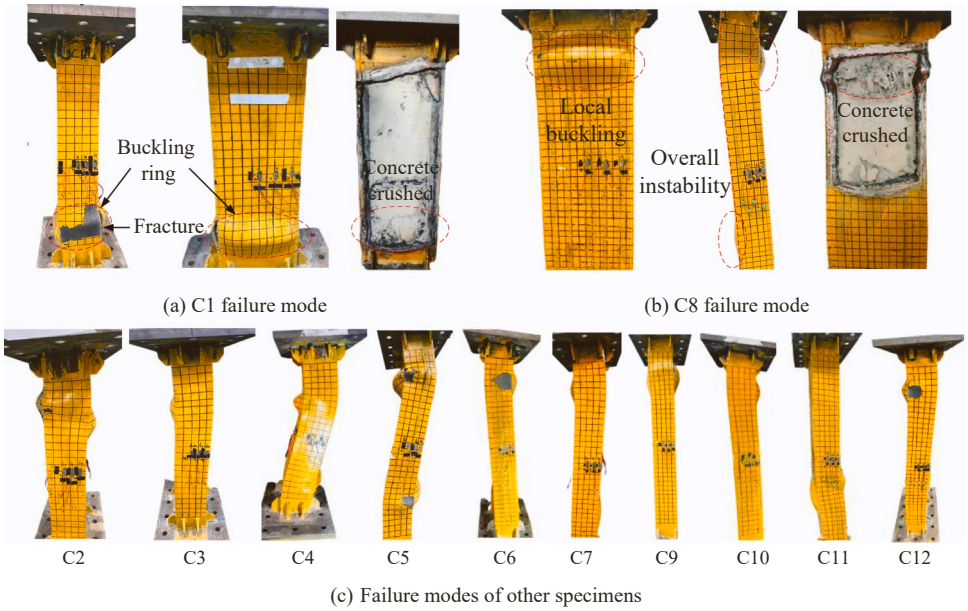

Fig. 2. Failure modes of all CFSTFCs.

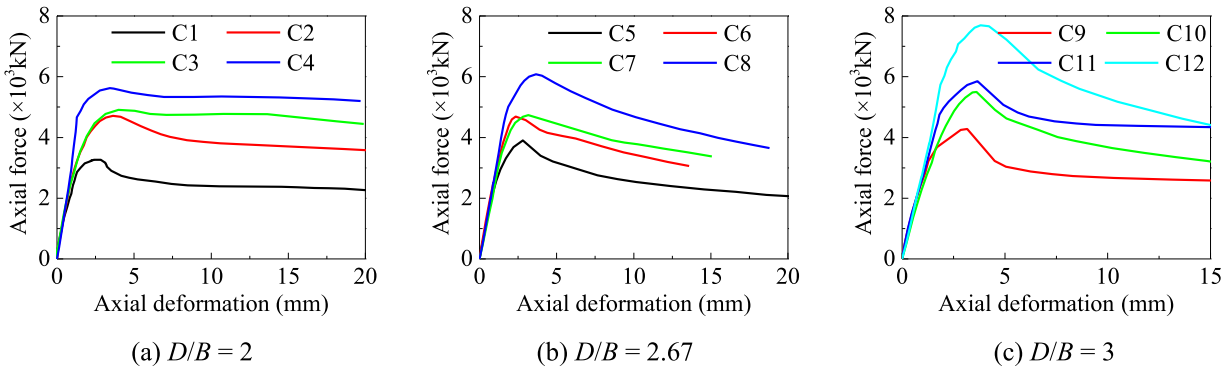

Fig. 3. Axial force-displacement curves of CFSTFCs.

Table 4
SI values of CFSTFCs.

Specimens	N_t (kN)	f_yA_s (kN)	f_cA_c (kN)	*SI*
C1	3265	2027.65	1134.07	1.03
C2	4714	3067.62	1084.72	1.14
C3	4912	3269.64	1036.32	1.14
C4	5625	4277.39	988.88	1.07
C5	3901	2494.85	1533.39	0.97
C6	4685	3781.02	1472.12	0.89
C7	4736	4037.16	1411.80	0.87
C8	6084	5290.99	1352.44	0.92
C9	4277	2728.45	1733.05	0.96
C10	5502	4137.72	1665.82	0.95
C11	5856	4420.92	1599.54	0.97
C12	7901	5797.79	1534.22	1.08

2.3. Test program

The test setup and data acquisition points are shown in Fig. 1. Four linear variable displacement transducers (LVDTs) were set on each side of the CFSTFCs to obtain the axial deformation of the CFSTFCs. The axial load was applied by the 1200 T loading system.

The force- and displacement-controlled methods were selected during loading. Before the applied axial force (N) was less than 70% of the predicted axial load-carrying capacity, the force-controlled method was used, and the increment of each stage was 10% of the predicted axial load-carrying capacity. Then, the loading method was changed to axial displacement-controlled, and each displacement amplitude was 0.5 mm. When the applied axial force-displacement curve exhibited a descending

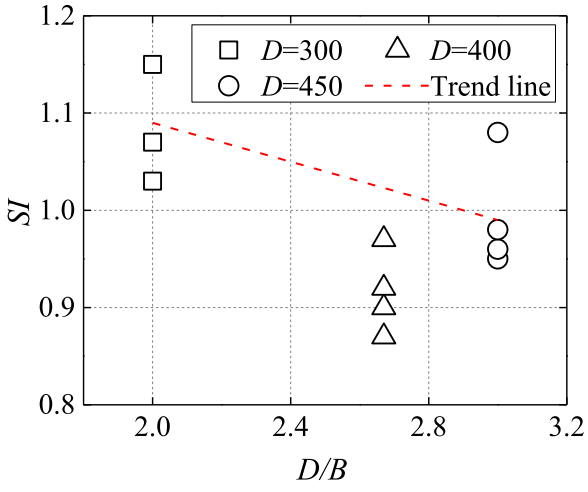

Fig. 4. *SI* value under different D/B.

Table 5
DI value of CFSTFCs.

Specimens	Δ_u	$\Delta_{85\%}$	*DI*
C1	2.8	5.1	1.82
C2	3.5	7.6	2.17
C3	4.0	23.2	5.80
C4	3.4	26.2	7.71
C5	2.3	3.7	1.61
C6	2.8	4.8	1.71
C7	3.6	6.9	1.92
C8	3.7	7.4	2.00
C9	3.2	3.4	1.06
C10	3.5	4.8	1.37
C11	3.7	5.1	1.38
C12	4.2	6.3	1.50

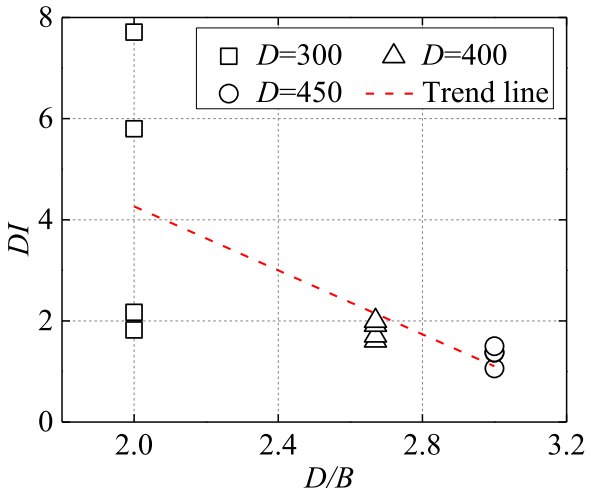

Fig. 5. *DI* value under different *D/B*.

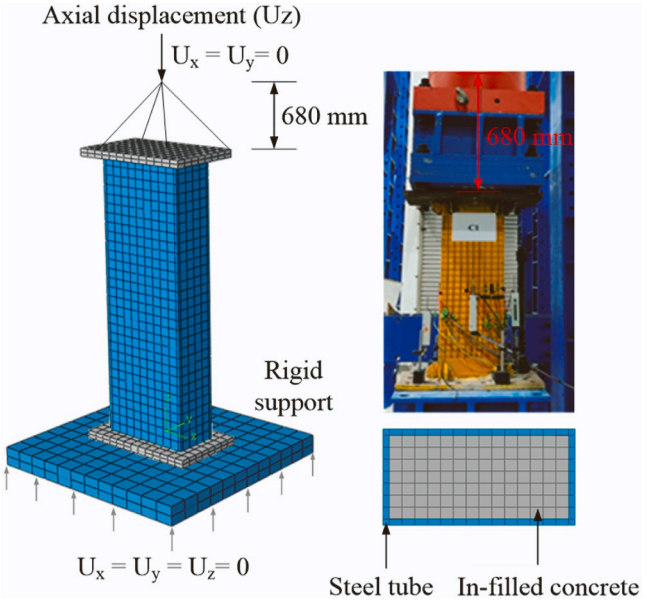

Fig. 6. FEM of CFSTFCs.

trend, the displacement amplitude of each stage was increased to 1 mm. The test stopped at an *N* value less than 80% of the ultimate axial load-carrying capacity (N_t) of CFSTFCs.

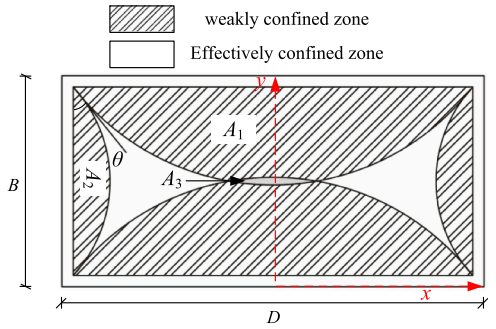

Fig. 7. Distribution of the effectively confined zone of in-filled concrete.

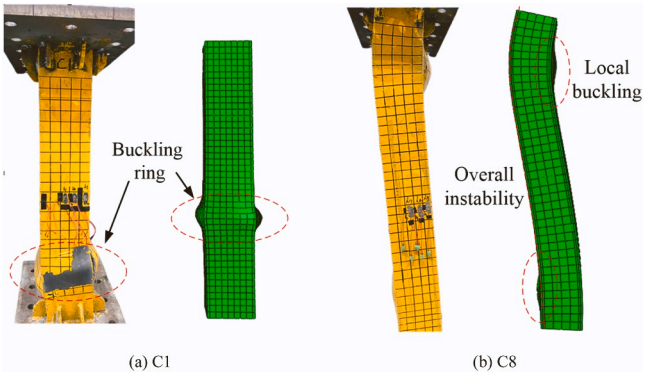

Fig. 8. Comparison of failure mode.

3. Test results and discussion

3.1. Failure modes

When $N < N_t$, no obvious deformation can be observed in the surface of CFSTFCs. At $N = N_t$, local buckling appeared on one side of the sectional height direction. Afterward, the failure progress of CFSTFCs can be divided into two types: (1) for specimens C1, C2, C9, and C11, a horizontal buckling ring appeared. With increasing axial displacement, the welding seam at the horizontal ring fractured. The first failure mode is shown in Fig. 2a. (2) For the other specimens, overall instability occurred, and buckling deformation can be found on the opposite surface. For the second failure type, no fractures can be observed at the welding seam. The second failure mode is shown in Fig. 2b. After the test, the steel plates of specimens C1 and C8 were cut. The in-filled concrete was crushed at the buckling position, as shown in Fig. 2a-b. The failure modes of the other specimens are shown in Fig. 2c. Generally, local buckling is a typical failure mode for CFSTFCs. As the thickness of the steel tube increased, the local stability was enhanced, and overall instability gradually occurred.

3.2. Axial force-displacement curves

The axial force-displacement curves of CFSTFCs are shown in Fig. 3. After $N = N_t$, with increasing applied axial displacement, the corresponding *N* value gradually decreased due to the buckling deformation of the steel tube and the crushing of the in-filled concrete. When the *t* value increased from 8 mm to 14 mm, the elastic stiffness of the CFSTFCs is improved. Under $D/B = 2.0$, at $t = 12$ mm and 14 mm, the slope at the descent phase of the axial force-displacement curves is significantly smaller than that of the CFSTFCs with $t = 8$ mm and 10 mm. However, this phenomenon is not obvious in CFSTFCs with $D/B = 2.67$ and 3.0. Specially, under $D/B = 3.0$. The axial force-displacement curves have a sudden drop after $N = N_t$.

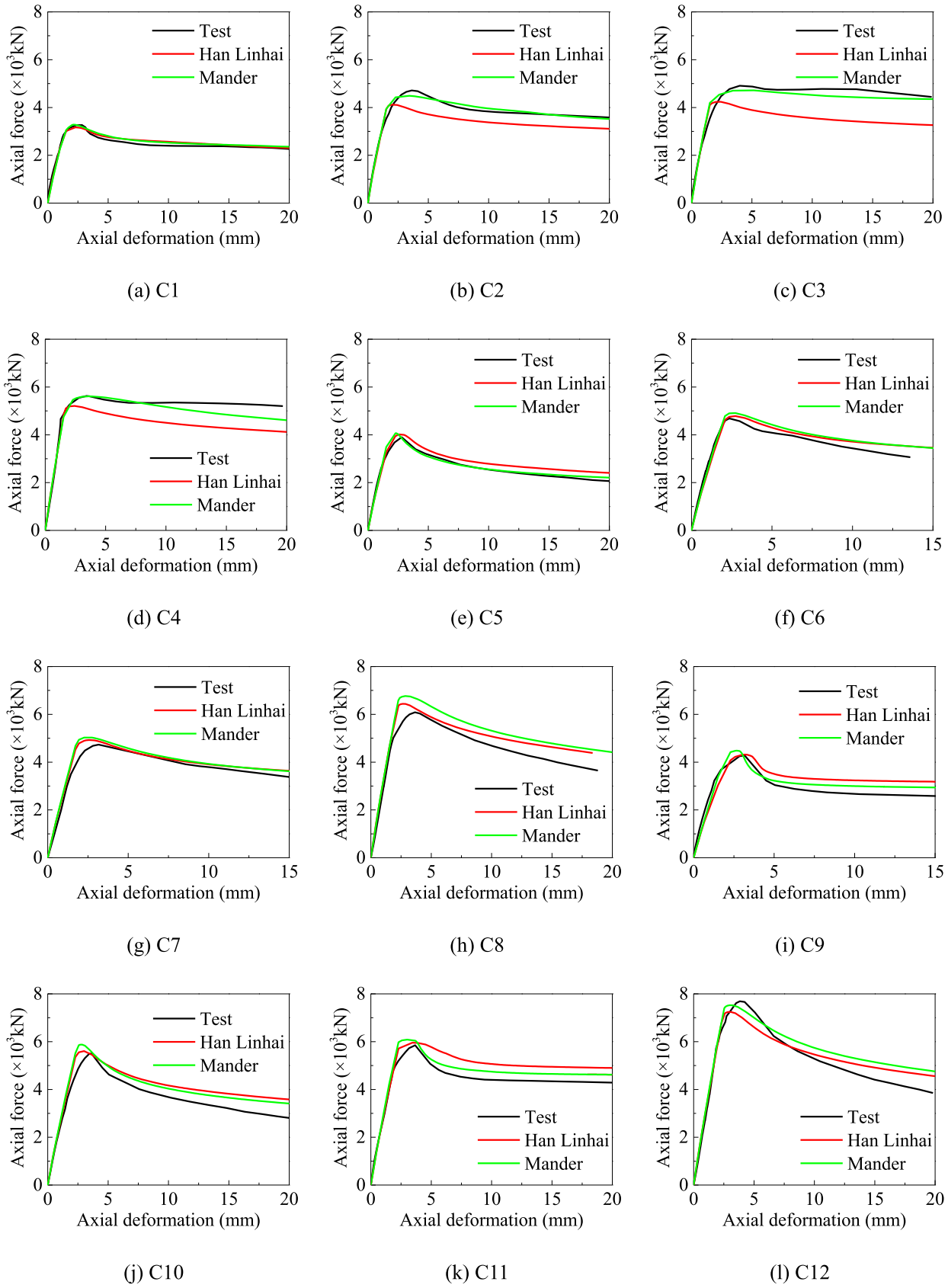

Fig. 9. Comparison of axial force-displacement curves.

Table 6
Error of N_t between the test and simulated results.

Specimens	N_t (kN)	Han Linhai model (kN)	Mander model (kN)	Error of Han Linhai model (%)	Error of Mander model (%)
C1	3265	3168.48	3280.74	-3.0	0.5
C2	4714	4119.88	4491.02	-12.6	-4.7
C3	4912	4237.09	4716.36	-13.7	-4.0
C4	5625	5207.67	5612.14	-7.4	-0.2
C5	3901	4016.09	4070.37	3.0	4.3
C6	4685	4784.24	4910.13	2.1	4.8
C7	4736	4925.01	5028.35	4.0	6.2
C8	6084	6439.77	6763.99	5.8	11.2
C9	4277	4316.57	4481.81	0.9	4.8
C10	5502	5605.69	5875.81	1.9	6.8
C11	5856	5954.03	6086.96	1.7	3.9
C12	7901	7242.65	7526.13	-8.3	-4.7

Table 7
Design method of N_c in different specifications.

Specifications	Design method
AISC 360	$N_c=A_sf_y+0.85A_cf_c'$
AS 5100.6	$N_c=0.9A_sf_y+0.6A_cf_c'$
CECS 159	$N_c=A_sf_y+A_cf_c$
GB 50936	$N_c=A_{sc}f_{sc}$ $A_{sc}=A_s+A_c$ $f_{sc}=(1.212+B\xi+C\xi^2)f_c$ $\xi=A_sf_y/A_cf_c$
DBJ/T 13–51	$N_c=(A_s+A_c)\cdot(1.18+0.85\xi)f_c$

3.3. Strength index

The strength index (*SI*) was introduced to evaluate the confinement effect from the steel tube to in-filled concrete. The *SI* value can be calculated by Eq. (1). A large *SI* value means that the compressive strength of the in-filled concrete is effectively enhanced by the confinement of the steel tube.

$$SI=\frac{N_t}{f_yA_s+f_cA_c} \tag{1}$$

where A_s is the sectional area of the steel tube and A_c is the total area of the in-filled concrete. The welding seams between the steel plates are not considered in calculating the A_s value.

The *SI* values of all CFSTFCs range from 0.87 to 1.14, as shown in Table 4. Generally, under the same *D/B*, with increasing *t*, the *SI* value is enhanced. However, this change is only approximately 10% from $t=8$ mm to $t=14$ mm. According to Fig. 4, the *SI* value gradually decreases with increasing *D/B*. When $D/B=2.67$ and 3.0, the average *SI* values of the C5-C8 specimens and C9-C12 specimens are smaller than 1.0, which means that the steel tube cannot provide effective confinement to improve the compressive strength.

3.4. Ductility index

The ductility index (*DI*) was defined as the ratio between the axial deformation at $N=N_t$ (Δ_u) and the axial deformation at $N=0.85N_t$ in the descent phase ($\Delta_{85\%}$). The *DI* value can be calculated by Eq. (2), which can be used to evaluate the deformation capacity of CFSTFCs.

$$DI=\frac{\Delta_{85\%}}{\Delta_u} \tag{2}$$

The Δ_u, $\Delta_{85\%}$ and *DI* values of all CFSTFCs are listed in Table 5. Under $D/B=2.0$, when the *t* value increased from 8 mm to 14 mm, the corresponding *DI* value increased by 323.6%. However, under $D/B=2.67$ and 3.0, the *DI* value is only increased by 24.2% and 41.5%, respectively. Thus, when $D/B=2.67$ and 3.0, increasing the thickness of the steel tube cannot effectively enhance the deformation capacity of CFSTFCs. Fig. 5 shows the relation between *DI* and the *D/B* value. With increasing *D/B*, the *DI* value gradually decreases. Under $t=14$ mm, when the *D/B* value increased from 2.0 to 3.0, the *DI* value decreased by 80.5%.

Based on the aforementioned analysis, at $D/B=2.67$ and 3.0, the confinement effect from the steel tube to in-filled concrete is significantly smaller than that of the specimens with $D/B=2.0$.

4. Finite element analysis

4.1. Finite element model

The finite element model (FEM) of CFSTFCs was established in ABAQUS software. The steel tube and in-filled concrete were built by C3D8R solid element. The friction coefficient between the steel tube and in-filled concrete was 0.25. The whole FEM and mesh size are shown in Fig. 6. The distance between the loading point and the top of CFSTFCs was 680 mm, which is the same as the actual loading system. A rigid support was set at the bottom of the CFSTFCs, and the friction coefficient between the CFSTFCs and rigid support was 0.3. An overall imperfection with 1/1000 of the total length of CFSTFCs[25] was applied in the FEMs.

4.2. Materials

The ideal elastic-plastic steel material was used in the steel tube. In the steel material, f_y and E_s were determined based on Section 2.2. The Mander[26] and Han Linhai[27] confined concrete models were selected to simulate the in-filled concrete and compare the accuracy of these two models in CFSTFCs. The Mander confined concrete model considers the shape of the CFSTFCs, and the compressive strength and ductility of concrete is improved by the confinement of the steel tube. The Han Linhai confined concrete model considers the steel ratio of the CFSTFCs to improve the confinement to concrete. The expression of the Mander and Han Linhai models can be seen in references [26,27]. For the Mander model, in calculating the effectively confined zone of CFSTFCs, the angle (θ) between the weakly confined zone and steel tube

Table 8
N_c in different specifications (unit: kN).

Specimens	N_t	AISC 360	AS 5100.6	CECS 159	ξ	GB 50936	DBJ/T 13–51
C1	3265	3042.07	2540.94	3161.41	1.79	3279.42	3619.94
C2	4714	4031.88	3440.34	4146.03	2.82	3920.37	4799.16
C3	4912	4290.69	3681.67	4399.74	3.25	3973.38	5281.67
C4	5625	5161.94	4474.04	5266.01	4.33	4127.97	6512.35
C5	3901	3866.46	3213.56	4027.83	1.63	4229.64	4582.01
C6	4685	5090.41	4325.75	5245.32	2.56	5087.33	6005.10
C7	4736	5289.91	4515.78	5438.48	2.85	5125.42	6444.38
C8	6084	6500.75	5615.84	6643.07	3.91	5528.68	8054.99
C9	4277	4278.65	3549.87	4461.03	1.57	4703.05	5064.74
C10	5502	5619.67	4768.45	5794.97	2.48	5665.11	6611.50
C11	5856	5840.64	4978.84	6008.97	2.76	5717.60	7086.69
C12	7901	7170.15	6186.74	7331.60	3.78	6211.32	8834.13

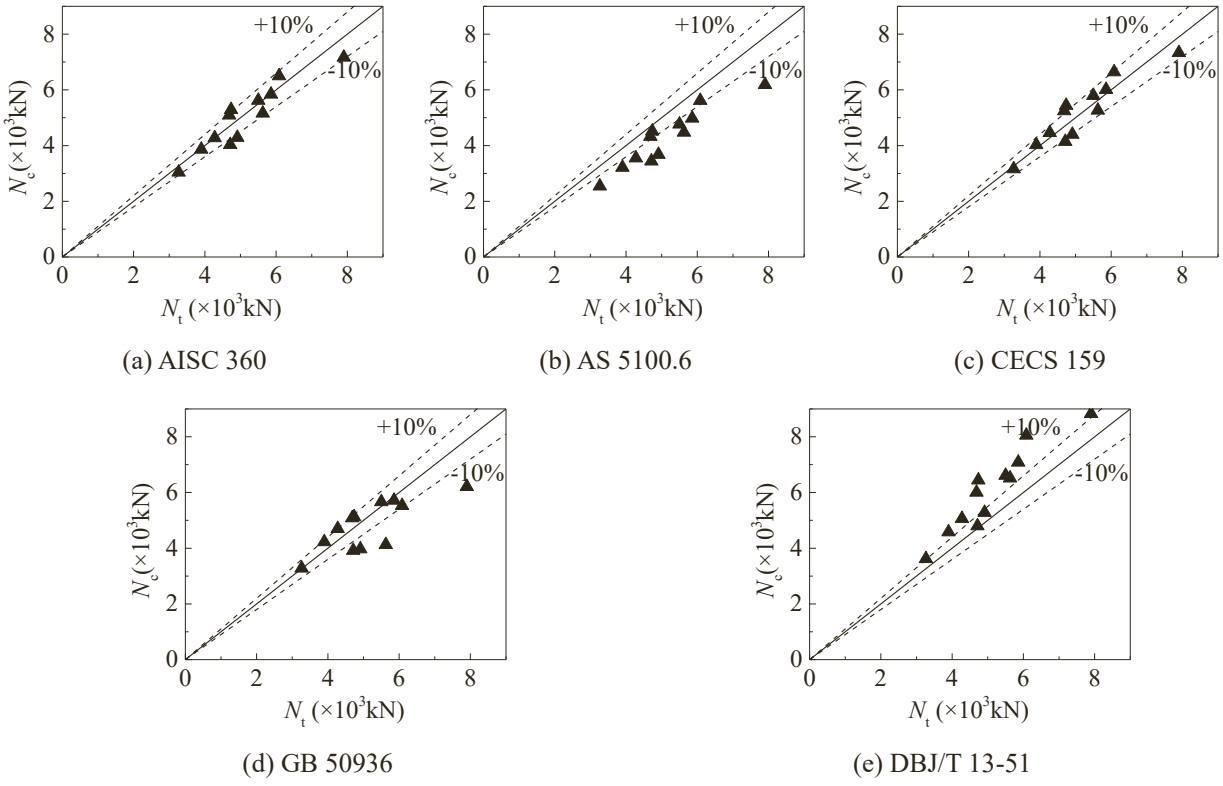

Fig. 10. Error between N_t and N_c.

was 45°[28]. For the CFSTFCs with $D/B = 2.67$ and 3.0, the weakly confined zone overlapped, as shown in Fig. 7. The actual area of the effectively confined zone (A_e) of CFSTFCs can be calculated by Eqs. (3–6).

$$A_1 = \frac{(D-2t)^2}{6} \tag{3}$$

$$A_2 = \frac{(B-2t)^2}{6} \tag{4}$$

$$A_3 = \int_{-0.5\sqrt{(D-2t)(D+2t-2B)}}^{0.5\sqrt{(D-2t)(D+2t-2B)}} \left(-\frac{1}{D-2t}x^2 + \frac{D-2t}{4} - \frac{B-2t}{2} \right) \mathrm{d}x \tag{5}$$

$$A_e = A_c - 2A_1 - 2A_2 + 2A_3 \tag{6}$$

where A_1 is the area of the weakly confined zone in the sectional height direction. A_2 is the area of the weakly confined zone in the sectional width direction. A_3 is the area of the overlapped weakly confined zone.

4.3. Comparison of the FE analysis and test results

4.3.1. Failure mode

Fig. 8 shows the comparison of the failure modes. Two different failure modes can be simulated by the established FEMs with Mander or Han Linhai confined concrete models. For the C1 specimen, the buckling ring appears in the steel tube of the FEM. Only the position has a small difference from the test results. For the C8 specimen, the overall instability and local buckling appear in the FEM, which has similar positions to the test results. Thus, the established FEM in ABAQUS software can reflect the failure mode of CFSTFCs.

4.3.2. Axial load-carrying capacity

The comparison of the axial force-displacement curves between the test and simulated results is shown in Fig. 9. Generally, the trend of the tested axial force-displacement curves can be reflected by the FEMs with the Mander or Han Linhai models. Because the Han Linhai model does not directly improve the compressive strength of the in-filled concrete under different steel ratio, the simulated N_t is less than that of the FEMs with the Mander model. Thus, the Han Linhai model provides a relatively conservative prediction of the axial load-carrying capacity. According to Table 6 and Fig. 9, under $D/B = 2.0$, when the thickness of the steel tube is larger than 10 mm, the N_t error of the Mander model is smaller, and the average N_t error is only − 2.1%. Under $D/B = 2.67$ and 3.0, the Han Linhai model shows relatively accurate results. The average N_t error is only 1.39%. Thus, when $D/B \geq 2.67$, the Han Linhai model is recommended to simulate the axial load-carrying capacity of CFSTFCs.

5. N_t prediction by different specifications

Five different specifications were chosen to calculate the axial load-carrying capacity of CFSTFCs and compared with the test results (N_t), which included AISC 360, AS 5100.6, CECS 159, GB 50936, and DBJ/T 13–51. The calculated axial load-carrying capacity was defined as N_c. The design method of different specifications is listed in Table 7. These specifications assume that the steel tube yields and that the in-filled concrete reaches compressive strength in calculating N_c. For AISC 360, AS 5100.6, and CECS 159, N_c is obtained by overlying the load carried by the steel tube and in-filled concrete. For GB 50936 and DBJ/T 13–51, the steel tube and in-filled concrete are combined, which can be seen as a composited material to calculate N_c. ξ in GB 50936 and DBJ/T 13–51 is the constraining factor to consider the confined effect of steel tubes on in-filled concrete. f_c' is the specified compressive strength of concrete, which is 0.8 f_{cu}.

The N_c calculation results are listed in Table 8. Compared with CECS 159, although the confined effect is considered in GB 50936, smaller N_c values will be obtained when $\xi > 2.0$. Different from GB 50936, the ξ value in DBJ/T 13–51 significantly improves the calculated N_c values. The error between GB 50936 and DBJ/T 13–51 is enhanced with increasing ξ, and the maximum error is 57.8%. However, when $\xi < 2.0$,

GB 50936 gives N_c values similar to those of CECS 159, and the maximum error for DBJ/T 13–51 is 10.4%. Thus, the design method provided in GB 50936 and DBJ/T 13–51 cannot be applied to calculate the axial load-carrying capacity of CFSTFCs with $\xi > 2.0$.

The error between N_c and N_t for different specifications is shown in Fig. 10. AS 5100.6 shows a small prediction of N_t, and the average error for AS 5100.6 is approximately 16%. In contrast, DBJ/T 13–51 provides a relatively higher prediction of N_t, and the average error is larger than 18%. Compared with GB 50936, the N_c values calculated by AISC-360 and CECS 159 are closer to N_t. The average errors for AISC-360 and CECS 159 are only 1.9% and 1.0%, respectively.

6. Conclusions

In this study, the influence of the aspect ratio (D/B) and the thickness of the steel tube on the axial compression performance of concrete-filled steel tube flat columns (CFSTFCs) was investigated by test and finite element analysis. The failure mode, axial load-carrying capacity, and ductility of CFSTFCs were analyzed. The accuracy of Mander and Han Linhai confined concrete models in simulating the compressive strength of in-filled concrete in CFSTFCs was studied. Finally, the prediction of the ultimate axial load-carrying capacity (N_t) of CFSTFCs in different specifications was compared. The following conclusions can be drawn:

(1) Two different failure modes exhibit in axial the compression test: (1) a horizontal buckling ring with welding seam fracture and (2) overall instability with local buckling in the sectional height direction.
(2) Under the same D/B, the compressive strength of in-filled concrete in CFSTFCs is enhanced with increasing steel tube thickness. However, the average strength index of CFSTFCs with $D/B = 2.67$ and 3.0 is smaller than 1.0, and the steel tube cannot provide effective confinement to improve the compressive strength.
(3) Under $D/B = 2.0$, the ductility index (DI) can be enhanced by 323.6% when the thickness of the steel tube increases from 8 mm to 14 mm. However, under $D/B = 2.67$ and 3.0, the DI value is only increased by 24.2% and 41.5%, respectively. Thus, the deformation capacity of CFSTFCs is deteriorated with increasing D/B. Using a thicker steel tube cannot effectively recover the deformation capacity of CFSTFCs.
(4) The Han Linhai confined concrete model is recommended to simulate the axial load-carrying capacity of CFSTFCs.
(5) AISC 360 and CECS 159 provide relatively accurate predictions of the N_t of CFSTFCs. AS 5100.6 gives small predictions, and DBJ/T 13–51 provides a relatively higher prediction. For GB 50936, if the constraining factor is larger than 2.0, a conservative prediction will be obtained.

Declaration of Competing Interest

The authors declare that they have no known competing financial interests or personal relationships that could have appeared to influence the work reported in this paper.

Acknowledgments

The research in this paper was financially supported by the National Natural Science Foundation of China (52378152), Anhui Provincial Key Research and Development Program (202104a07020022) and Fundamental Research Funds for the Central Universities (PA2023GDSK0068). This support is gratefully acknowledged.

References

[1] Ibañez C, Hernández-Figueirido D, Piquer A. Effect of steel tube thickness on the behaviour of CFST columns: Experimental tests and design assessment. Eng Struct 2021;230:111687.
[2] Han Linhai. Tests on stub columns of concrete-filled RHS sections. J Constr Steel Res 2002;50:353–72.
[3] Yang Youfu, Han Linhai. Experiments on rectangular concrete-filled steel tubes loaded axially on a partially stressed cross-sectional area. J Constr Steel Res 2009; 65:1617–30.
[4] Cai Yancheng, Su Meini, Chen Xuerui, et al. High strength steel square and rectangular tubular stub columns infilled with concrete. J Constr Steel Res 2021; 179:106536.
[5] Du Yansheng, Chen Zhihua, Yu Yujie. Behavior of rectangular concrete-filled high-strength steel tubular columns with different aspect ratio. Thin–Walled Struct 2016;109:304–18.
[6] Lo SH, Kwan AKH, Ouyang Y, et al. Finite element analysis of axially loaded FRP-confined rectangular concrete columns. Eng Struct 2015;100:253–63.
[7] Ouyang Y, Kwan AKH. Finite element analysis of square concrete-filled steel tube (CFST) columns under axial compressive load. Eng Struct 2018;156:443–59.
[8] Faxing Ding, Lei Fu, Zhiwu Yu, et al. Mechanical performances of concrete-filled steel tubular stub columns with round ends under axial loading. Thin-Walled Struct 2015;97:22–34.
[9] Hassanein MF, Patel VI. Round-ended rectangular concrete-filled steel tubular short columns: FE investigation under axial compression. J Constr Steel Res 2018; 140:222–36.
[10] Liu Ziao, Liu Hongbo, Chen Zhihua, et al. Structural behavior of cold-formed thick-walled rectangular steel columns. J Constr Steel Res 2018;147:277–92.
[11] Liu Dongyu, Liu Hongbo, Chen Zhihua, et al. Structural behavior of extreme thick-walled cold-formed square steel columns. J Constr Steel Res 2017;128:371–9.
[12] EC4 EN. -1, Design of Composite Steel and Concrete Structures, Part 1.1. General Rules and Rules for Buildings, European Committee for. Stand, Bruss 1994-1:2004.
[13] AS 5100.6. Bridge design, part6: steel and composite construction. Sydney, Australia, 2004.
[14] CECS 159. Technical Specification for Structures with Concrete-filled Rectangular Steel Tube Members. Beijing: China Planning Press,; 2004.
[15] DBJ/T 13-51. Technical Specification for Concrete-Filled Steel Tubular Structures. Beijing: China Planning Press,; 2010.
[16] GB 50936. Technical Code for Concrete Filled Steel Tubular Structures. Beijing: China Architecture & Building Press,; 2014.
[17] ANSI/AISC 360-16. Specification for Structural Steel Buildings. Chicago, USA: American Institute of Steel Construction (AISC),; 2016.
[18] Zhang Lei, Mao Chenxiang, Gang Lixiao, et al. Experimental study on CFNRST members under combined compression and bending. J Constr Steel Res 2020;167: 105950.
[19] Zhang Lei, Yang Shuanglong, Fu Bo, et al. Behavior and design of concrete-filled narrow rectangular steel tubular (CFNRST) stub columns under axial compression. J Build Eng 2021;37:102166.
[20] Yang Shuanglong, Zhang Lei, Zhang Jiawei, et al. Seismic behavior of concrete-filled wide rectangular steel tubular (CFWRST) stub columns. J Constr Steel Res 2022;196:107402.
[21] Wang Yunhe, Guo Lanhui, Li Hongda. L-shaped steel-concrete composite columns under axial load: Experiment, simulations and design method. J Constr Steel Res 2021;185:106871.
[22] Zheng Yongqian, Zeng Shaoxi. Design of L-shaped and T-shaped concrete-filled steel tubular stub columns under axial compression. Eng Struct 2020;207:110262.
[23] Han Jianhong, Shu Ganping, Qin Ying, et al. Experimental seismic behavior of double skin composite wall with steel truss. J Constr Steel Res 2021;184:106776.
[24] GB/T 50107. Standard for evaluation of concrete compressive strength. Beijing: China Architecture & Building Press,; 2010.
[25] Tao Zhong, Wang Zhibin, Yu Qing. Finite element modelling of concrete-filled steel stub columns under axial compression. J Constr Steel Res 2013;89:121–31.
[26] Mander JB, Priestley MJN, Park R. Theoretical stress-strain model for confined concrete. J Struct Eng 1988;114(8):1804–26.
[27] Han Linhai, Yao Guohuang, Zhao Xiaoling. Tests and calculations for hollow structural steel (HSS) stub columns filled with self-consolidating concrete (SCC). J Constr Steel Res 2005;61:1241–69.
[28] Yang Yuanlong, Wang Yuyin, Fu Feng, et al. Static behavior of T-shaped concrete-filled steel tubular columns subjected to concentric and eccentric compressive loads. Thin-Walled Struct 2015;95:374–88.